Energy-Based Mechanistic Approach for Crack Growth Characterization of Asphalt Binder

Hui Li , Xue Luo , Weizhuo Yan , Yuqing Zhang

PII: S0167-6636(20)30179-4
DOI: https://doi.org/10.1016/j.mechmat.2020.103462
Reference: MECMAT 103462

To appear in: *Mechanics of Materials*

Received date: 20 February 2020
Revised date: 6 May 2020
Accepted date: 6 May 2020

Please cite this article as: Hui Li , Xue Luo , Weizhuo Yan , Yuqing Zhang , Energy-Based Mechanistic Approach for Crack Growth Characterization of Asphalt Binder, *Mechanics of Materials* (2020), doi: https://doi.org/10.1016/j.mechmat.2020.103462

The nonlinear viscoelastic critical strain level separating from damage is determined

A theoretical formula of the crack length is derived based on a pure mechanical method

A relationship between crack growth rate and material properties is established

Paris' law parameters are independent of strain levels and temperatures

Energy-Based Mechanistic Approach for Crack Growth Characterization of Asphalt Binder

Hui Li
College of Civil Engineering and Architecture
Zhejiang University
866 Yuhangtang Road, An-zhong Bldg.
Hangzhou 310058, Zhejiang, China
Email: huili94@zju.edu.cn
Xue Luo[1,2]
(corresponding author)
1. College of Civil Engineering and Architecture
Zhejiang University
866 Yuhangtang Road, An-zhong Bldg.
Hangzhou 310058, Zhejiang, China
2. National Engineering Laboratory of Highway Maintenance Technology, Changsha University of Science & Technology, Changsha 410114, Hunan, China
Phone: (86) 571-88206542
Email: xueluo@zju.edu.cn
Weizhuo Yan
College of Civil Engineering and Architecture
Zhejiang University
866 Yuhangtang Road, An-zhong Bldg.
Hangzhou 310058, Zhejiang, China
Email: yanwz14@zju.edu.cn
Yuqing Zhang
Aston Institute of Materials Research
Aston University
Aston Triangle, Birmingham, B4 7ET, U.K.
Phone: +44 (0) 121-204-3391
Email: y.zhang10@aston.ac.uk

ABSTRACT

The cohesive cracking within asphalt binders has a significant influence on fatigue cracking resistance of asphalt pavements. To more clearly understand the mechanism and accurately characterize the process of the cohesive cracking occurring within the asphalt binder. An energy-based mechanics (EBM) approach is applied to determine crack length and the pseudo J-integral is adopted to calculated crack growth rate in this study. First, a critical strain level separating nonlinear viscoelasticity from damage is determined based on statistical analysis approach, and result indicates that 0.7% is a critical nonlinear strain level for unmodified asphalt binder. Then, crack length of asphalt binders is derived based on a torque equilibrium equation and two energy

balance equations, as well as crack length is measured and verified based on an image processing method. It is found that contact regions in cracked area of the asphalt binder are formed when performing a strain-controlled rotational shear load. There are two change stages of contact regions which first increase and then decrease with increase of loading time. Next, crack growth rate is formulated based on the pseudo J-integral *Paris' law* equation which considering nonlinear viscoelasticity. Linear relationship between crack growth rate and the function of material properties (such as shear modulus, phase angle) in double logarithm scale is proven and experimentally verified. *In addition, Paris' law parameters* (*n* and *A*) associated with crack growth rate are determined. Results show they are independent on strain levels and temperatures. For example, six *Paris' law parameter*s *n* of unmodified asphalt binder are approximately equal to 1.10 at 5%, 6%, 7% of strain level when test temperatures are 15°C and 20°C. They are inherent material properties for the asphalt binder.

Keywords: Fatigue cracking; Asphalt binder; Nonlinear viscoelasticity*; Paris' law;* Crack growth rate.

1 Introduction

Fatigue cracking resistance of asphalt mixtures plays a critical role in determining the fatigue cracking resistance of asphalt pavements. Fatigue cracking of asphalt mixtures is commonly caused by cohesive failure within the asphalt binder. Therefore, accurately characterizing and understanding the fatigue behavior of asphalt binder is of great significance in guiding the design of asphalt mixtures and extend the service life for asphalt pavement. Many fatigue characterization indicators have been proposed for asphalt binders, which are generally classified as: (1) empirical indicators; (2) indirect mechanical indicators; (3) direct mechanical indicators, like crack length and crack growth rate.

Many empirical indicators have been proposed as fatigue failure criterions for asphalt binders. Such as, a 50% loss in stiffness and pseudo-stiffness criterion are established (Hicks et al.,1993; Kim et al.,1997). The peak of phase angle is defined as the critical fatigue failure point during fatigue tests (Reese, 1997). The peak of $S \times N$

(S is the stiffness, N is the number of loading cycles) is considered a fatigue failure point (Rowe and Bouldin, 2000). In addition, a fatigue factor denoted as $|G^*|sin$ ($|G^*|$ is shear modulus and is the phase angle) is proposed to characterize the fatigue behavior of asphalt binder in the Strategic Highway Research Program (SHRP) (Anderson & Kennedy, 1993). However, some researchers suggest that empirical indicators are not well correlated with the fatigue life of asphalt mixtures and asphalt pavements (Zhou et al.,2013).

In order to improve the usage of the empirical indicators. Indirect mechanical indicators have been proposed to reflect the fatigue behavior of asphalt binders from the perspective of dissipated energy ratio (DER) (Anderson et al.,2001; Martono et al., 2007; Wang et al., 2016) and the ratio of dissipated energy change (RDEC) (Shen et al., 2006; Shen et al., 2010; Subhy et al., 2017). These dissipated energy criterions are superior to the empirical criterions, because they are derived based on mechanical principles and material properties. However, these indirect mechanical indicators not provide explanations to the fatigue behavior and fatigue mechanisms for asphalt binders.

To better directly quantify the physical process of fatigue cracking. Some researchers focused on studying direct mechanical indicators of asphalt binders which include crack length and crack growth rate. Such as, crack length calculated by the theoretical formula and measured by the image processing method have been compared during a shear fatigue cracking process (Hintz and Bahia, 2013, Shan et al., 2017). In these studies, it is not rigorous for asphalt binders to use the linear viscoelastic constitutive equation at undamaged state to derive crack length at damage stage. For this reason, a damage mechanics-based crack length model has been established for asphalt binders under a rotational shear fatigue load (Zhang and Gao, 2019, Li et al., 2020). However, materials properties (such as shear modulus, phase angle) under linear viscoelastic condition are selected to calculated crack length under damaged condition.

In addition, there are some studies on the crack growth rate for asphalt binders. The relationship between energy release rate and crack growth rate is fitted and

analyzed for asphalt binders (Hintz and Bahia, 2013, Gao et al., 2020), which indicated the fitting model parameters are independent on the magnitude of loading amplitude. However, the energy release rate of asphalt binders is calculated without taking the nonlinear viscoelasticity into consideration. Therefore, the viscosity of asphalt binders is incompletely eliminated, which make it impossible to accurately determine the model parameters of crack growth rate. Besides, Safaei and Castorena (2017) commented that the effect of material nonlinearity has been ignored in most of asphalt binders damage analysis and attributed all material integrity losses to damage for the sake of simplicity.

As a result, in order to further understand the physical process of fatigue cracking and better overcome the problems above-mentioned. It is necessary to fundamentally study the crack length and crack growth rate of asphalt binders by taking the nonlinear viscoelasticity into consideration under a rotational shear fatigue load. Hence, the objective of this work is that determining the crack length and crack growth rate based on a purely mechanical method, which can directly characterize the fatigue cracking behavior of asphalt binders.

This study is organized as follows. Firstly, test materials and methods are elaborated. Secondly, using the statistical analysis approach to determinate critical strain levels separating linear viscoelasticity and nonlinear viscoelasticity from damage. Thirdly, shear strain model, shear stress model and energy items are established under a rotational shear fatigue load. Then, a formula of crack length for asphalt binders is derived based on the EBM approach and verified by an image processing method. Next, the pseudo J-integral is obtained by taking the nonlinear viscoelasticity into account and crack growth rate is established based on the pseudo J-integral *Paris' law*. In addition, *Paris' law parameters associated with crack growth rate are determined at* different oscillation shear strain levels and temperatures. Finally, a summary section concludes this study with the main results.

2 Materials and Laboratory Tests

2.1 Materials

Two types of asphalt binders commonly used in China are selected in this study, which represent unmodified asphalt binders and SBS modified asphalt binders. Three replicates for each type of the asphalt binder are tested based on the method in the specification (China, 2010a; 2010b; 2011; 2014). The requirement and measured average results of basic properties (penetration, softening point and ductility) of the unmodified asphalt binder and SBS modified asphalt binder are showed in Table 1. Basic properties of asphalt binders can meet the requirement in the specification.

Table 1. Basic properties of unmodified asphalt binders and SBS modified asphalt binders

Properties	Unit	Unmodified asphalt binders			SBS modified asphalt binders		
		Method	Requirement	Result	Method	Requirement	Result
Penetration at 25℃	0.1mm	T 0604 (China, 2011)	40-60	56	GB/T 4509 (China, 2010b)	60-80	74
Softening point	℃	T 0606 (China, 2011)	*60*	88.4	GB/T 4507 (China, 2014)	44-57	47.3
Ductility at 5℃	cm	T 0605 (China, 2011)	*20*	36.5	GB/T 4508 (China, 2010a)	*100*	>150

2.2. Equipment and Sample Preparation

Discovery Hybrid Rheometer (Figure 1a) from TA Instruments is adopted to conduct tests for asphalt binders. In this study, an 8-mm diameter parallel plate geometry is employed by forming a specimen 8 mm in diameter, 2 mm in height. Specimens are prepared by pouring the hot asphalt binder that can flow into the silicon rubber mould (Figure 1b), and cool them to room temperature for a period time. Then, the specimen is removed by flexing the rubber mould and adhered to the lower parallel plate by gently pressing the top surface of the pellet. After that, the upper parallel plate is lowered close to the asphalt binder until the gap is equate to the trim gap *(2050μm)* and then rock the rotating lever (Figure 1c). A heated trimming tool is employed to trim the excess asphalt

binder around the edges of the plates so that the asphalt binder is the same as the outer diameter of the plates. When the trimming step is complete, the upper parallel plate is lowered to the target gap (2000μm), which is shown in Figure 1d. T*he extra 50μm can* ensure that a proper lateral bulge is formed at the outside face of the asphalt binder specimen. Finally, to avoid uneven temperature distribution throughout the entire asphalt binder specimen volume, the specimen is heated to the testing temperature and keep it for 5 min before loading.

a. Discovery Hybrid Rheometer

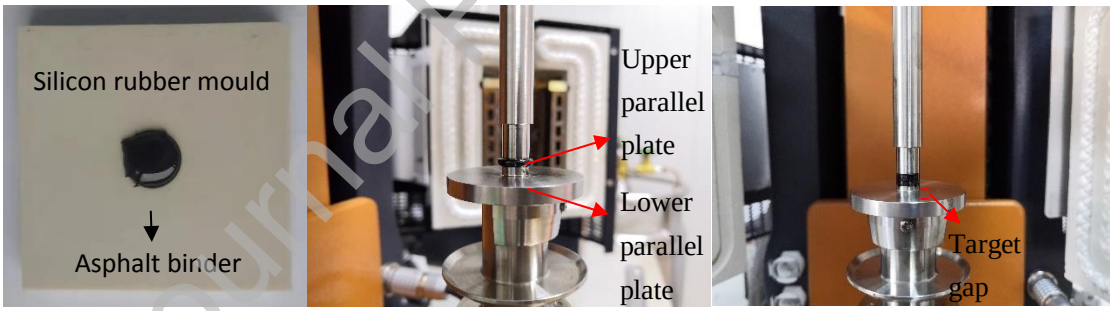

b. Asphalt binder specimen c. Trim gap d. Target gap

Figure 1. Equipment and sample preparation of the test

2.3 Test Methods

In this study, three types of tests including linear amplitude sweep test, time sweep test under low and high oscillation shear strain level are performed. Two types of asphalt binders (unmodified asphalt binders and SBS modified asphalt binders) are tested. Besides, all tests are conducted at two temperatures (15°C and 20°C) and one loading frequency (10 Hz).

(1) Linear amplitude sweep test

The purpose of linear amplitude sweep test is to approximate the range of undamaged oscillation shear strain levels and the nonlinear critical point. When performing linear amplitude sweep test, the oscillation shear strain levels is ranged from 0.1% to 30% linearly. The unmodified asphalt binder as an example, and results of shear modulus/phase angle are determined from linear amplitude sweep test at 20°C and 10 Hz, which are shown in Figure 2. It is found that the shear modulus and phase angle remain basically unchanged in linear region (within about 1%), that is the sample is undamaged. If the oscillation shear strain level is being in nonlinear region, for example 5%, the sample will be damaged.

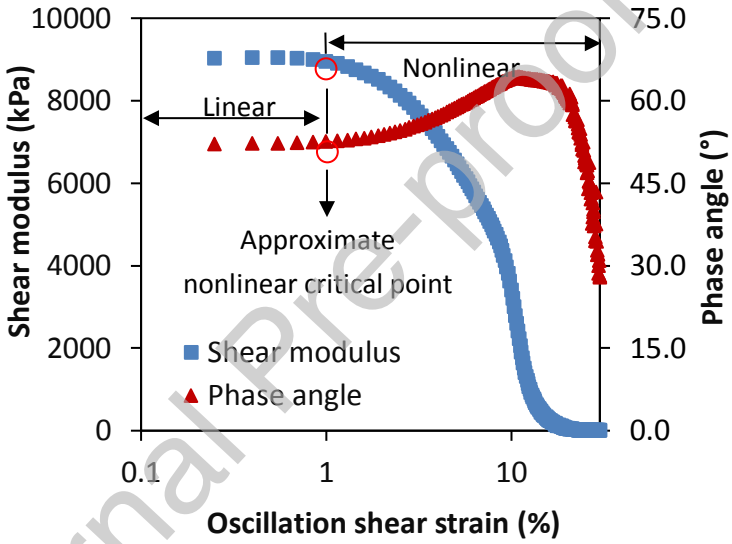

Figure 2. Results of shear modulus/phase angle are determined from linear amplitude sweep test for the unmodified asphalt binder at 20°C and 10 Hz

(2) Time sweep test under low oscillation shear strain level

Although more data of shear modulus or phase angle at one oscillation shear strain level can be obtained from linear amplitude sweep test. There are only ten loading cycles for each oscillation shear strain level in the linear amplitude sweep test. In this way, only an approximate nonlinear critical point of oscillation shear strain level can be obtained (about 1% for unmodified asphalt binder in Figure 2). Hence, a series of time sweep tests under low oscillation shear strain level are performed to accurately determine linear and nonlinear critical points in this study. First, the initial oscillation shear strain level (Level 1) of time sweep test is selected to be 0.1% to assure that the sample is

undamaged. Then, oscillation shear strain level is increased with an increment of o.1% until the sample is damaged (Level i), and the protocol is shown in Figure 3. Each time sweep test lasts for 600s, that is 6000 loading cycles. If a time sweep test is completed, the sample will rest for 1000s to assure that the linear viscoelastic and nonlinear viscoelastic deformation completely recover.

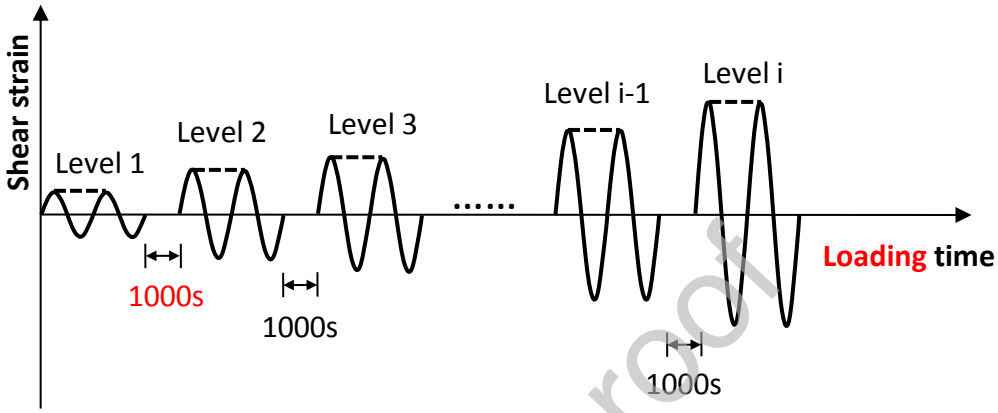

Figure 3. A series of time sweep tests protocol at low oscillation shear strain levels

(3) Time sweep test under high oscillation shear strain level

The aim of time sweep test under high oscillation shear strain level is to calculate crack length and crack growth rate. When the critical nonlinear viscoelastic strain level is determined, two consecutive time sweep tests are performed on the same asphalt binder specimen. First, time sweep test under critical nonlinear viscoelastic strain level is performed to determine the critical material properties (shear modulus and phase angle). Then, the sample rest for 1000s. Next, time sweep tests at high oscillation shear strain levels (5%, 6%, 7% for unmodified asphalt binders and 7%, 8%, 9% for SBS modified asphalt binders) are conducted to obtain the shear modulus and phase angle for the asphalt binder. Figure 4 shows relationship between shear modulus/phase angle of the unmodified asphalt binder and loading time when the time sweep test is performed at 5%, 20°C and 10 Hz. As we can see from Figure 4 that the shear modulus decreases, phase angle increases to the peak and then decreases with increase of loading time. Besides, the value of phase angle fluctuates at the later loading stage.

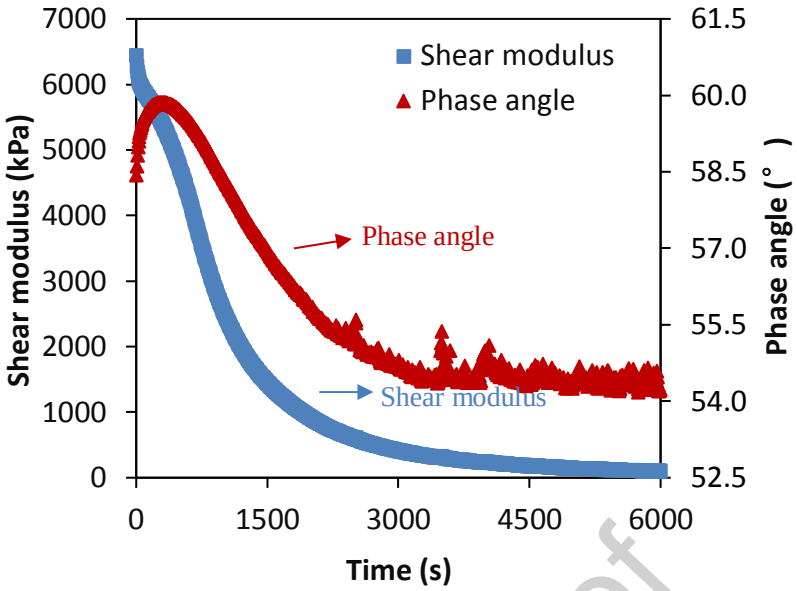

Figure 4. Relationship between shear modulus/phase angle of the unmodified asphalt binder and loading time when the time sweep test is performed at 5%, 20°C and 10 Hz

3 Determination of Linear and Nonlinear Viscoelastic Critical Strain Levels

After conducting a series of time sweep tests, the linear viscoelastic and nonlinear viscoelastic critical strain levels of asphalt binders will be determined. The procedure is as follows:

1) Analyze the change rules of shear modulus and phase angle of time sweep tests under different oscillation shear strain levels; and

2) Determine linear and nonlinear viscoelastic critical strain levels based on statistical analysis of test data.

3.1 Analysis of Shear Modulus and Phase Angle of Asphalt Binders

Figure 5 shows typical relationship of shear modulus and phase angle versus oscillation shear strain level of asphalt binders. The undamaged region and the damaged region are separated by the nonlinear viscoelastic critical point (Point B and D in Figure 5). The undamaged region consists of the linear viscoelastic region and the nonlinear viscoelastic region, separated by Point A and C in Figure 5. Therefore, in order to determine the critical points (A and C, B and D), a series of time sweep tests shown in

Figure 3 is performed to obtain the shear modulus and phase angle for the asphalt binder at different oscillation shear strain levels.

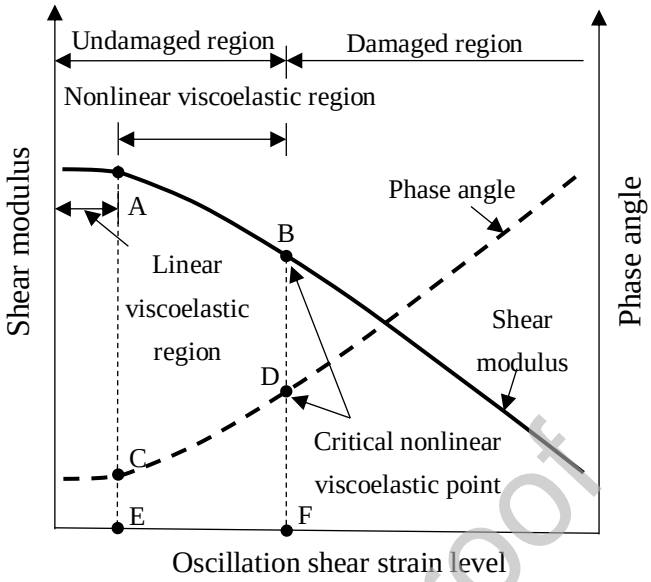

Figure 5. Typical relationship of shear modulus and phase angle versus oscillation shear strain level of asphalt binders

The unmodified asphalt binder is analyzed as an example. Plots of shear modulus and phase angle versus loading time or oscillation shear strain level at 20°C and 10 Hz are generated and given in Figure 6. Two observations can be obtained from Figure 6: (1) the magnitude of shear modulus and phase angle remain approximately constant with the increase of the loading time at relatively low oscillation shear strain level (0.1% in Figure 6a and 0.5% in Figure 6b). However, the shear modulus decreases and the phase angle increases with the increase of the loading time at relatively high oscillation shear strain level (1.0% in Figure 6c); and (2) Figure 6d shows that the shear modulus and phase angle basically unchanged when oscillation shear strain level is ranged from 0.1 % to 0.3%. However, when oscillation shear strain level is ranged from 0.3 to 0.9%, the shear modulus decreases and the phase angle increases with the increase of oscillation shear strain level. Therefore, the linear viscoelastic critical strain level of the unmodified asphalt binders is between 0.1% and 0.5%, as well as the nonlinear viscoelastic critical strain level is between 0.5% and 1.0%.

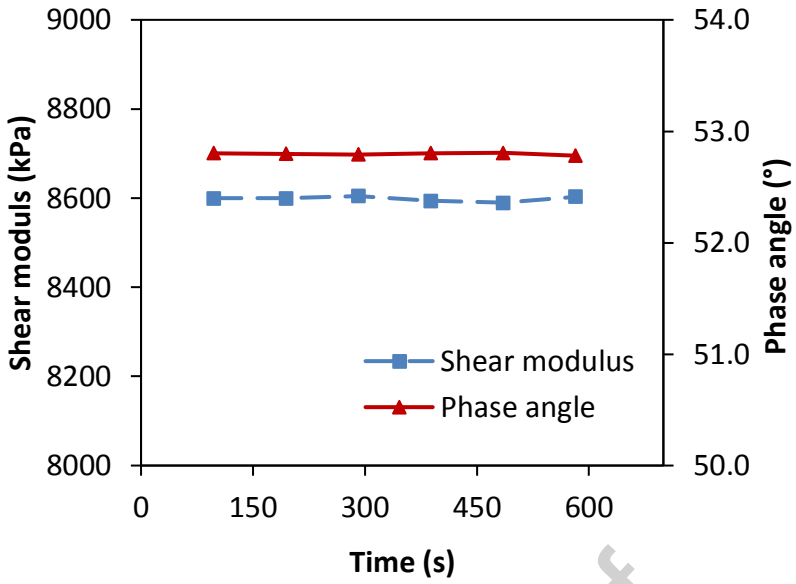

a. Shear modulus and phase angle versus loading time (oscillation shear strain level is 0.1%)

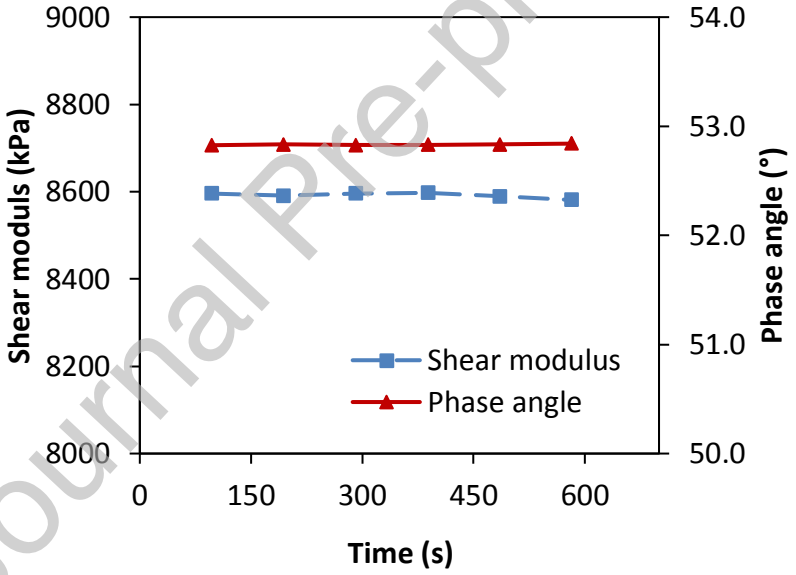

b. Shear modulus and phase angle versus loading time (oscillation shear strain level is 0.5%)

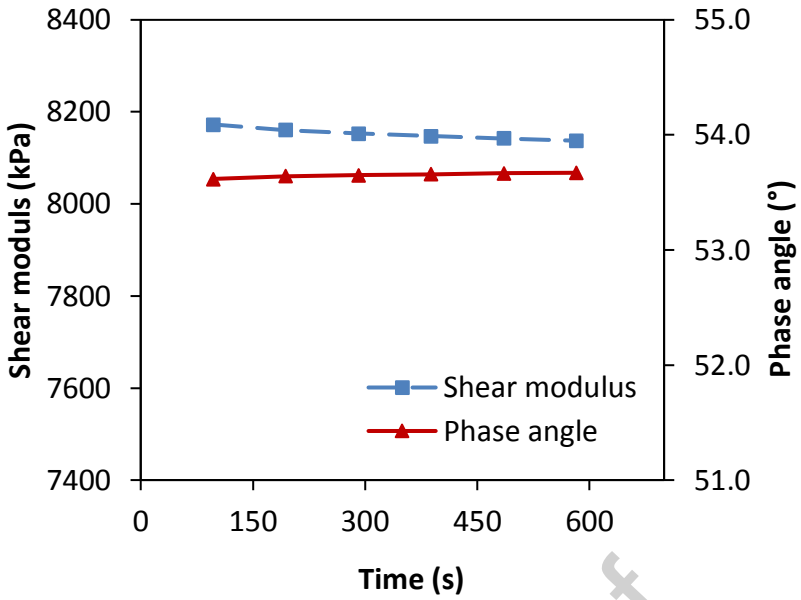

c. Shear modulus and phase angle versus loading time (oscillation shear strain level is 1.0%)

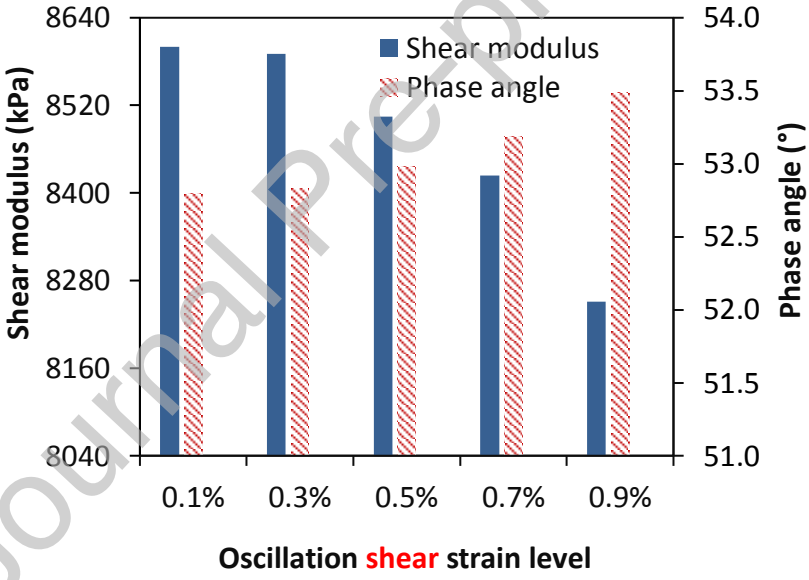

d. Shear modulus and phase angle versus oscillation shear strain level

Figure 6. Shear modulus and phase angle of the unmodified asphalt binder at 20°C and 10 Hz

3.2 Statistical Analysis of Test Data

To accurately determine the linear viscoelastic and nonlinear viscoelastic critical levels of asphalt binders, statistical analysis is performed on the shear modulus and phase angle obtained from a series of time sweep tests. In this study, shear modulus and phase angle of unmodified asphalt binders at 20°C and 10 Hz are taken as an example, and

the same analysis can be performed on other conditions or other asphalt binders.

First, the hypotheses have been selected for the shear modulus and phase angle. The null hypothesis H_0, the alternative hypothesis H_1 are shown in Table 2. Then, sampling procedure is performed. For hypothesis I and II, the sample population of shear modulus and phase angle contains six groups, and 50s in each group. For hypothesis III and IV, the six mean values of shear modulus and phase angle in six groups at different oscillation shear strain levels are selected as sample population. Specifically, the six groups are the 50s-100s, 150s-200s, 250s-300s, 350s-400s, 450s-500s and 550s-600s. Next, based on the Analysis ToolPak in Microsoft Excel, One-Way ANOVA tests are performed for hypothesis I and II, and t-tests are performed for hypothesis III and IV. In addition, the variables of hypothesis I, II, III and IV presented in Table 2 are included: (1) $\left|G^*\right|_{Ni}, \delta_{Ni}$ are a group of shear modulus and phase angle; N (N=50) is the number of sample and i (i=6) is the number of groups; and (2) $\overline{\left|G^*\right|}_k, \overline{\delta}_k$ are group mean value of shear modulus and phase angle; k and j (k=0.1%,0.2%,0.3%; j=0.2%,0.3%,0.4%; $k < j$) are oscillation shear strain level.

Table 2. Null hypothesis and alternative hypothesis for statistical hypothesis testing

Hypothesis	Null hypothesis H_0	Alternative hypothesis H_1	Statistical test
I	$\left\|G^*\right\|_{N1} = \left\|G^*\right\|_{N2} = \left\|G^*\right\|_{N3} = \cdots = \left\|G^*\right\|_{Ni}$	At least one $\left\|G^*\right\|_{Ni}$ differs from the rest	One-Way ANOVA
II	$\delta_{N1} = \delta_{N2} = \delta_{N3} = \cdots = \delta_{Ni}$	At least one δ_{Ni} differs from the rest	
III	$\overline{\left\|G^*\right\|}_k \geq \overline{\left\|G^*\right\|}_j$	$\overline{\left\|G^*\right\|}_k < \overline{\left\|G^*\right\|}_j$	t-test
IV	$\overline{\delta}_k \leq \overline{\delta}_j$	$\overline{\delta}_k > \overline{\delta}_j$	

Finally, results of One-Way ANOVA tests and t-tests are analyzed. On one hand, the

values of the F-statistic and the critical F-statistic of One-Way ANOVA test at a 95% confidence level under different oscillation shear strain levels are calculated, which are listed in Table 3. When the oscillation shear strain level is ranged from 0.1% to 0.7%, the F-statistic values of the shear modulus and phase angle are smaller than the critical F-statistic. As a result, the null hypotheses H_0 cannot be rejected. However, when the oscillation strain level exceeds 0.7%, the null hypothesis H_0 is rejected. Consequently, oscillation shear strain level of the nonlinear viscoelastic critical point (point B and D in Figure 4) can be determined between 0.7% and 0.8%. For convenience, the threshold nonlinear oscillation shear strain level is taken 0.7%.

Table 3. Values of F-statistic and critical F-statistic of One-Way ANOVA test at 95% confidence level

Material property	F-statistic								Critical F-statistic
	0.1%	0.2%	0.3%	0.4%	0.5%	0.6%	0.7%	0.8%	
$\left\|G^*\right\|_{Ni}$	0.639	0.635	1.056	0.329	0.431	0.148	0.146	10.03	2.214
δ_{Ni}	0.669	1.456	0.945	0.164	0.247	0.122	0.109	40.31	

On the other hand, through a series of t-tests performed at a 95% confidence level, the values of the t-statistic and the critical t-statistic of t-tests are calculated and listed in Table 4. The absolute values of the t-statistic are smaller than their corresponding critical t-statistics when two pairs are 0.1% versus 0.2%, 0.1% versus 0.3%, 0.2% versus 0.3%. However, when two pairs are 0.1% versus 0.4%, 0.2% versus 0.4%, 0.3% versus 0.4%, the analysis results are opposite. Hence, 0.3% is taken as threshold linear oscillation shear strain level of the linear viscoelastic critical point (point A and C in Figure 5). The shear modulus and phase angle at the nonlinear viscoelastic critical point are denoted as $\left|G^*\right|_{NLVE}$ and δ_{NLVE} in this study, respectively.

Table 4. Values of t-statistic and critical t-statistic of t-test at 95% confidence level

Material property	t-statistic						Critical t-statistic
	0.1% versus 0.2%	0.1% versus 0.3%	0.2% versus 0.3%	0.1% versus 0.4%	0.2% versus 0.4%	0.3 versus 0.4 %	
$\overline{\lvert G^* \rvert}_k$	-2.084	-0.287	1.954	17.92	23.66	15.64	2.145
$\bar{\delta}_k$	-1.932	-2.022	0.478	-26.39	-22.12	-35.1	

4. Establishment of Expression of Energy Items for Asphalt Binders

When the nonlinear viscoelastic critical strain level has been determined and two consecutive time sweep tests have been performed on the asphalt binder, crack length and crack growth rate of the asphalt binder can be calculated. However, the shear strain, shear stress and energy of asphalt binders should be modeled first. Therefore, this section contains the following two aspects:

1) Establish the shear strain and shear stress model for asphalt binders; and
2) Determine the energy items for asphalt binders.

4.1 Determination of Shear Strain and Shear Stress Model for Asphalt Binders

Cracks of asphalt binders will form at the edge of cylindrical specimen and gradually expand to the loading center as the loading time increases under a relatively large strain-controlled rotational shear load. The shear strain, shear stress and energy distribution in the intact material are certainly different from those in the apparent material (including the volume of the crack) because of the presence of cracks. However, there is a close relationship with strain, stress and energy between the intact material and the apparent material. For instance, the torque applied to the intact material should be equal to the torque applied in the apparent material. In this study, the shear strain, shear stress *and energy applied in the intact material defined as the "true shear stress", "true shear strain" and "true energy", respectively.* By comparison, that applied in the apparent *material is defined as the "apparen*t shear stress*", "apparent shear strain" and "apparent energy"*, respectively.

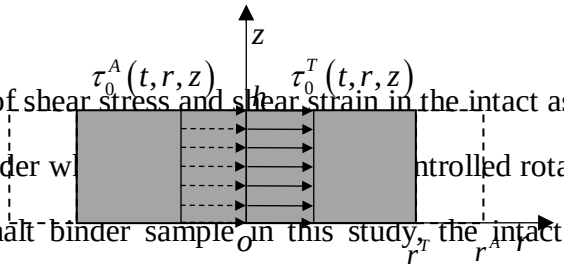

Figure 7. Distribution of shear stress and shear strain in the intact asphalt binder and the apparent asphalt binder w[illegible]ntrolled rotational shear load

For the cylindrical asphalt binder sample in this study, the intact material and the apparent material are called the intact asphalt binder and the apparent asphalt binder, respectively. Figure 7 shows distribution of shear stress and shear strain in the intact asphalt binder and the apparent asphalt binder when performing a strain-controlled rotational shear load. It is worth[illegible] shear stress and shear strain are linear function along the *r* dir[illegible]ion along the *z* direction. The apparent radius r^A is equal to th[illegible] the cylindrical asphalt binder specimen. However, the true rad[illegible] to crack growth.

Next, the shear strain model and shea[illegible]el of the apparent asphalt binder and the intact asphalt binder can be established. For the apparent asphalt binder, the apparent shear strain at any loading time and any point is modeled by:

$$\gamma^A(t,r,z)=\gamma_0^A(t_0,r,z)\sin(\omega t)=\frac{\theta_0^A}{h}r\sin(\omega t) \tag{1}$$

where $\gamma^A(t,r,z)$ is the apparent shear strain; $\gamma_0^A(t_0,r,z)$ is the apparent shear strain amplitude at the loading time t_0, a given radius r and a given height z, $0\le r\le r^A$, $0\le z\le h$; θ_0^A is the amplitude of apparent rotational angle; h is the height of the sample; ω is loading frequency and t is the loading time in a loading period $[t_0,t_0+2\pi/\omega]$.

The apparent shear stress is modeled by the sinusoidal waves, which is presented as below:

$$\tau^A(t,r,z)=\tau_0^A(t_0,r,z)\sin(\omega t+\delta^A)=\frac{r}{r^A}\tau_0(t_0,r^A,h)\sin(\omega t+\delta^A) \tag{2}$$

in which $\tau^A(t,r,z)$ is the apparent shear stress; $\tau_0^A(t_0,r,z)$ is the apparent shear stress amplitude at the loading time t_0, a given radius r and a given height z; δ^A is the apparent phase angle.

The apparent shear modulus can be calculated by:

$$\left|G^{*A}\right| = \frac{\tau_0^A\left(t_0, r, z\right)}{\gamma_0^A\left(t_0, r, z\right)} \tag{3}$$

Similarly, for the true asphalt binder, the true shear strain at any loading time and any point is modeled by:

$$\gamma^T\left(t, r, z\right) = \gamma_0^T\left(t_0, r, z\right)\sin\left(\omega t\right) = \frac{\theta_0^T}{h} r \sin\left(\omega t\right) \tag{4}$$

where $\gamma^T\left(t, r, z\right)$ is the true shear strain; $\gamma_0^T\left(t_0, r, z\right)$ is the true shear strain amplitude at the loading time t_0, a given radius r and a given height z, $0 \le r \le r^T$; θ_0^T is the amplitude of true rotational angle.

The true shear stress is modeled by the following equation:

$$\tau^T\left(t, r, z\right) = \tau_0^T\left(t_0, r, z\right)\sin\left(\omega t + \delta\right) = \frac{r}{r^T}\tau_0\left(t_0, r^T, h\right)\sin\left(\omega t + \delta^T\right) \tag{5}$$

in which $\tau^T\left(t, r, z\right)$ is the true shear stress; $\tau_0^T\left(t_0, r, z\right)$ is the true shear stress amplitude at the loading time t_0, a given radius r and a given height z; δ^T is the true phase angle.

The true shear modulus can be calculated by:

$$\left|G^{*T}\right| = \frac{\tau_0^T\left(t_0, r, z\right)}{\gamma_0^T\left(t_0, r, z\right)} \tag{6}$$

4.2 Determination of Energy Items for Asphalt Binders

When the shear strain model and the shear stress model of the intact asphalt binder and the apparent asphalt binder are established, the energy items can be determined. First, the hysteresis loop of a loading cycle at one point in the asphalt binder is shown in Figure 8. There are three hysteresis loops: (1) apparent shear stress vs. apparent shear strain (from point O through points M, N, Q to point O); (2) apparent shear stress vs. apparent shear pseudo strain (from point E through points L, F, P to point E); and (3) true shear stress vs. true shear strain (*from point O through points M, N, Q* to point *O*).

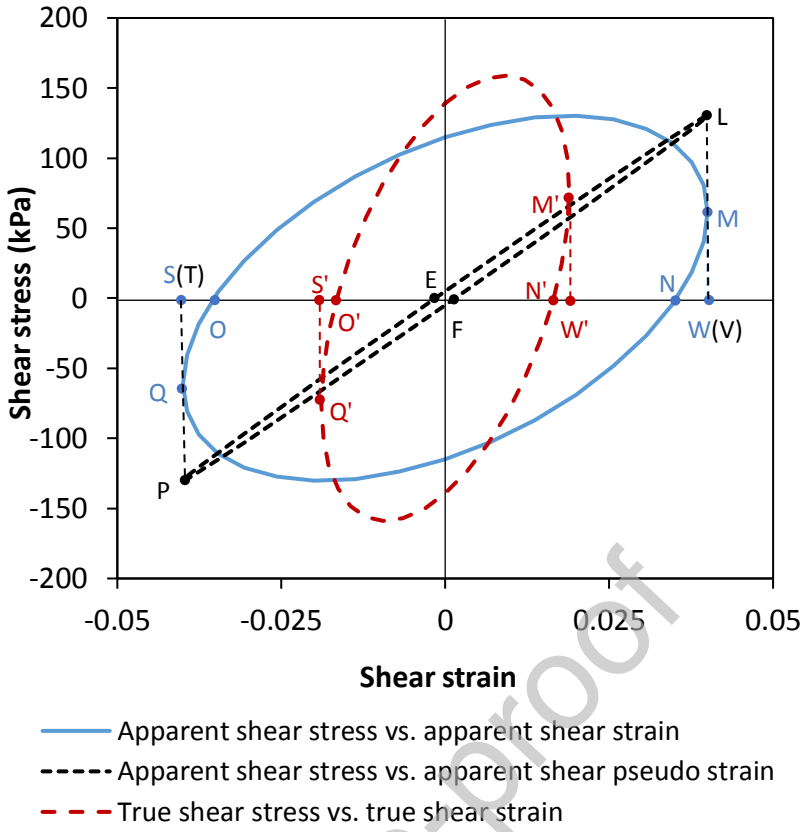

Figure 8. Hysteresis loop of a loading cycle at one point in the asphalt binder when performing a strain-controlled rotational shear test

As shown in Figure 8, the apparent asphalt binder is storing strain energy from point O to M, the amount of the energy during this period is the closed area OMW. From point M to N, the apparent asphalt binder is recovering strain energy, and the amount of energy is the area MWN. From point N to Q, the amount of stored strain energy during this period is the closed area NQS. From point Q to O, the apparent asphalt binder is recovering strain energy, and the amount of the energy is the area QSO. Consequently, the amount of dissipated strain energy (overcoming the viscous resistance and developing damage) is calculated by deducting the recovered strain energy (area MWN and area QSO) from the stored strain energy (area OMW and area NQS) in this period. In addition, when the viscous of the apparent asphalt binder is removed, the amount of dissipated pseudo strain energy (developing damage) during this period is the closed area ELFPE. Similar analysis is applied to the intact asphalt binder in Figure 8. Table 5 summarizes dissipated and recoverable strains energy in a loading cycle.

Table 5. Dissipated and recoverable strains energy in a loading cycle

State	Area	Energy	Lower limit	Upper limit
Apparent asphalt binder	OMNQO	$DSE^A(t_0,r,z)$	t_0	t_0+2 /
	MWN	$RSE^A(t_0,r,z)$	$t_0+(\ -\ ^A)/$	t_0+ /
	QSO	$RSE^A(t_0,r,z)$	$t_0+(2\ -\ ^A)/$	t_0+2 /
	ELFPE	$DPSE^A(t_0,r,z)$	t_0	t_0+2 /
True asphalt binder	$O\ M\ N\ Q\ O$	$DSE^T(t_0,r,z)$	t_0	t_0+2 /
	$M\ W\ N$	$RSE^T(t_0,r,z)$	$t_0+(\ -\ ^T)/$	t_0+ /
	$Q\ S\ O$	$RSE^T(t_0,r,z)$	$t_0+(2\ -\ ^T)/$	t_0+2 /

As a result, the apparent dissipated strain energy (DSE^A) can be formulated by the area of hysteresis loop OMNQO, which is calculated as follows:

$$DSE^A\left(t_0,r,z\right)=\int_{t_0}^{t_0+2\pi/\omega}\tau^A\left(t,r,z\right)d\gamma^A\left(t,r,z\right) \tag{7}$$

where $DSE^A\ (t_0,r,z)$ is DSE^A at the loading time t_0, at a given radius r ($0\le r\le r^A$) and a given height z.

The apparent recovered strain energy (RSE^A) can be represented by the area of MWN and QSO, giving the following equation:

$$RSE^A\left(t_0,r,z\right)=\int_{t_0+\left(\pi-\delta^A\right)/\omega}^{t_0+\pi/\omega}\tau^A\left(t,r,z\right)d\gamma^A\left(t,r,z\right)+\int_{t_0+\left(2\pi-\delta^A\right)/\omega}^{t_0+2\pi/\omega}\tau^A\left(t,r,z\right)d\gamma^A\left(t,r,z\right) \tag{8}$$

where $RSE^A\ (t_0,r,z)$ is RSE^A at the loading time t_0, at a given radius r ($0\le r\le r^A$) and a given height z.

The apparent pseudo dissipated strain energy ($DPSE^A$) is represented by the area of hysteresis loop ELFPE, which is calculated by:

$$DPSE^A\left(t_0,r,z\right)=\int_{t_0}^{t_0+2\pi/\omega}\tau^A\left(t,r,z\right)d\gamma_R^A\left(t,r,z\right) \tag{9}$$

where $DPSE^A\ (t_0,r,z)$ is $DPSE^A$ at the loading time t_0, at a given radius r ($0\le r\le r^A$) and a given height z; $\gamma_R^A\left(t,r,z\right)$ is the apparent shear pseudo strain.

Similarly, the true energy items can be determined. The area of hysteresis loop $O\ M\ N\ Q\ O$ stand for the true dissipated strain energy (DSE^T), which is calculated by:

$$DSE^T\left(t_0,r,z\right)=\int_{t_0}^{t_0+2\pi/\omega}\tau^T\left(t,r,z\right)d\gamma^T\left(t,r,z\right) \tag{10}$$

in which $DSE^T(t_0,r,z)$ is DSE^T at the loading time t_0, at a given radius r ($0\le r\le r^T$) and a given height z.

The area of hysteresis loop MWN and QSO stand for the true recovered strain energy (RSE^T), which gives:

$$RSE^T\left(t_0,r,z\right)=\int_{t_0+\left(\pi-\delta^T\right)/\omega}^{t_0+\pi/\omega}\tau^T\left(t,r,z\right)d\gamma^T\left(t,r,z\right)+\int_{t_0+\left(2\pi-\delta^T\right)/\omega}^{t_0+2\pi/\omega}\tau^T\left(t,r,z\right)d\gamma^T\left(t,r,z\right) \tag{11}$$

in which $RSE^A(t_0,r,z)$ is RSE^A at the loading time t_0, at a given radius r ($0\le r\le r^T$) and a given height z.

5 Determination of Crack Length and Crack Growth Rate for Asphalt Binders

The nonlinear viscoelastic critical point and energy items of asphalt binders have been determined and modeled based on the analysis of the section 3 and section 4, respectively. Next, the crack length and crack growth rate of asphalt binders can be analyzed by taking nonlinear viscoelasticity into account. The specific procedure is contained as below:

1) Derive a formula of crack length for asphalt binders based on the EBM approach and verify the formula by an image processing method; and
2) Establish crack growth rate by using the pseudo J-integral as well as determining *Paris' law parameters for asphalt binders*.

5.1 Formulation and Verification of Crack Length for Asphalt Binders

Step 1: Formulation of crack length

An EBM approach was established and applied in our previous studies to determine the evolution of damage or healing of asphalt mixtures in a pure mechanistic manner (Luo et al., 2014a; 2014b; 2020). Based on the demand of this research, the mathematical forms of the EBM approach include a torque equilibrium principle and two energy balance principles of asphalt binders can be listed:

$$T^A\left(t_0\right)=T^T\left(t_0\right) \tag{12}$$

$$DSE^A\left(t_0\right)=DSE^T\left(t_0\right) \tag{13}$$

$$RSE^A(t_0) = RSE^T(t_0) \tag{14}$$

where $T^A(t_0)$ is the apparent torque at loading time t_0; $T^T(t_0)$ is the true torque at loading time t_0; $DSE^A(t_0)$ is the total DSE^A at loading time t_0; $DSE^T(t_0)$ is the total DSE^T at loading time t_0; $RSE^A(t_0)$ is the total RSE^A at loading time t_0; $RSE^T(t_0)$ is the total RSE^T at loading time t_0.

First, the torque and total energy items for the entire volume of the asphalt binder are obtained. For the apparent asphalt binder, integration of the $DSE^A(t_0,r,z)$ (Equation 7), the $DSE^A(t_0)$ is obtained as below:

$$DSE^A(t_0) = \iiint_{V^A} DSE^A(t_0, r, z)\, dV \tag{15}$$

where V^A is the entire volume of the apparent asphalt binder sample.

Integration of $RSE^A(t_0)$ (Equation 8) gives:

$$RSE^A(t_0) = \iiint_{V^A} RSE^A(t_0, r, z)\, dV \tag{16}$$

The apparent torque is calculated as below:

$$T^A(t_0) = \int_0^{r^A} \tau_0^A(t_0, r, z) \cdot 2\pi r \cdot dr \cdot r = \frac{1}{2}\tau_0^A(t_0, r^A, z)\pi\left(r^A\right)^3 \tag{17}$$

in which $\tau_0^A(t_0, r^A, z)$ is the apparent shear stress amplitude at the loading time t_0, at a given radius r^A and a given height z.

Similarly, for the intact asphalt binder, the $DSE^T(t_0)$ is integrated by $DSE^T(t_0,r,z)$ (Equation 9), yields:

$$DSE^T(t_0) = \iiint_{V^T} DSE^T(t_0, r, z)\, dV \tag{18}$$

where V^T is the entire volume of the intact asphalt binder sample.

The $RSE^T(t_0)$ (Equation 10) can be determined by the following equation:

$$RSE^T(t_0) = \iiint_{V^A} RSE^T(t_0, r, z)\, dV \tag{19}$$

The true torque can be determined by:

$$T^T(t_0) = \frac{1}{2}\tau_0^T(t_0, r^T, z)\pi\left(r^T\right)^3 \tag{20}$$

in which $\tau_0^T(t_0, r^T, z)$ is the true shear stress amplitude at the loading time t_0, at a

given radius r^T and a given height *z*.

Then, substitute Equation 15 and Equation 18 into Equation 13, the following expression is obtained:

$$\frac{\pi^2 \sin\delta^A \left[\tau_0^A\left(t_0, r^A, z\right)\right]^2 \left(r^A\right)^2 h}{2\left|G^{*A}\right|} = \frac{\pi^2 \sin\delta^T \left[\tau_0^T\left(t_0, r^T, z\right)\right]^2 \left(r^T\right)^2 h}{2\left|G^{*T}\right|} \tag{21}$$

According to Equation 13, Equation 14, Equation 15, Equation 16, Equation 18 and Equation 19, the following equation can be established:

$$\frac{DSE^A\left(t_0\right)}{RSE^A\left(t_0\right)} = \frac{DSE^T\left(t_0\right)}{RSE^T\left(t_0\right)} = \frac{2\pi \sin\delta^T}{\left(\sin\delta^T\left(\pi - 2\delta^T - \sin\left(2\delta^T\right)\right) - 2\cos^3\left(\delta^T\right)\right)} \tag{22}$$

Based on Equation 12, Equation 17 and Equation 20, the following expression can be obtained:

$$\frac{1}{2}\tau_0^A\left(t_0, r^A, z\right)\pi\left(r^A\right)^3 = \frac{1}{2}\tau_0^T\left(t_0, r^T, z\right)\pi\left(r^T\right)^3 \tag{23}$$

Next, combine Equation 21, Equation 22 with Equation 23, the true radius r^T for the asphalt binder sample can be solved as below:

$$r^T = \left[\frac{\left|G^{*A}\right|}{\left|G^{*T}\right|}\right]^{1/4} r^A \tag{24}$$

An empirical formula $r(t) = const * \left[\left|G^*\right|\right]^{1/4}$ is adopted to calculate the actual shear radius *r(t)* when performing a time sweep test on the polystyrene and polyethylene (KM Mattes et al., 2008). In this study, a theoretical formula (Equation 24) is proposed based on a pure mechanical method. The true radius can be determined by true shear modulus, apparent shear modulus and apparent radius of the asphalt binder sample. The initial shear modulus of the time sweep test under high oscillation shear strain level is selected as the true shear modulus. In this way, the crack length of asphalt binders is formulated as follows:

$$c = r^A - r^T \tag{25}$$

where *c* is the crack length of asphalt binders.

Results of unmodified asphalt binders are analyzed as an example. Figure 9a and Figure 9b present calculated true radius and calculated crack length of unmodified

asphalt binders at 20°C and 10Hz. It can be seen from Figure 9b that crack length increases and growth rate decreases with the increase of loading time at three oscillation shear strain levels (5%,6%,7%). Because the increment of dissipated strain energy which promotes crack growth decreases with increase of loading time, when a strain-controlled rotational shear load is performed. In addition, larger oscillation shear strain level can increase crack length under the same loading time and loading conditions, which is caused by the larger increment of dissipated strain energy.

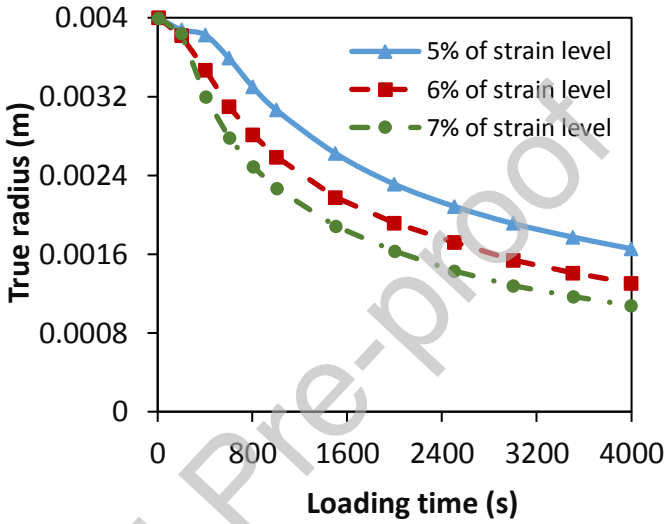

a. Calculated true radius at three oscillation shear strain levels (5%,6%,7%)

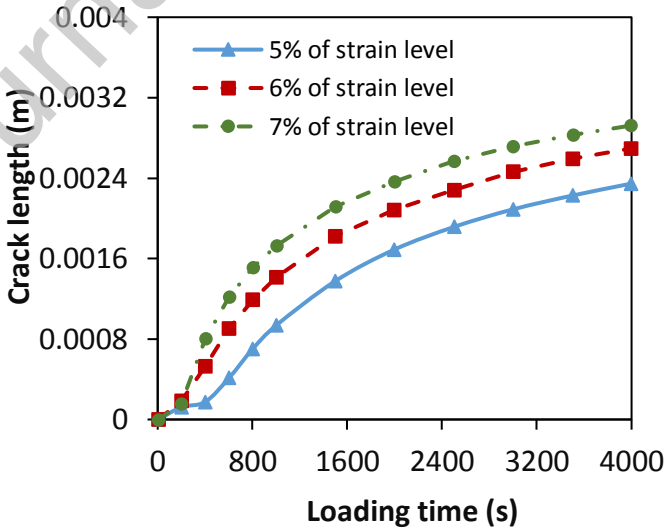

b. Calculated crack length at three oscillation shear strain levels (5%,6%,7%)

Figure 9. Calculated true radius and crack length of unmodified asphalt binders at 20°C and 10 Hz

Step 2: Verification of true radius and crack length

In this study, the image processing is performed to validate the calculated results of Equation 24 and Equation 25. The asphalt binder surface shows different characteristics at different areas after performing the time sweep test under high oscillation shear strain level, and an area equivalent method is used to determine the true radius and crack length. Figure 10a presents equivalent diagram of uncrack area, crack area and flow area of the asphalt binder. The outermost area is called flow area which is caused by unstable flow (Keentok and Xue, 1999). T*he "factory roof" crack in the middle region* is called cracked area caused by oscillation fatigue shear load. The center nondestructive region is called uncracked area. The true radius r^T, apparent radius r^A and crack length c of the asphalt binder can be measured from the image in Figure 10a. Besides, many contact regions in cracked area of the asphalt binder are formed when performing a strain-controlled rotational shear load, which are presented by numerous red lines in Figure 10b.

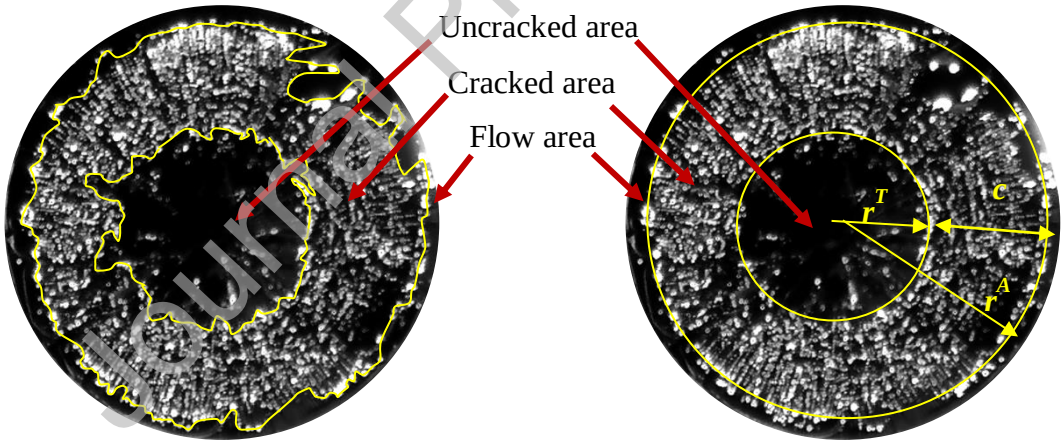

a. Equivalent diagram of uncrack area, crack area and flow area of the asphalt binder

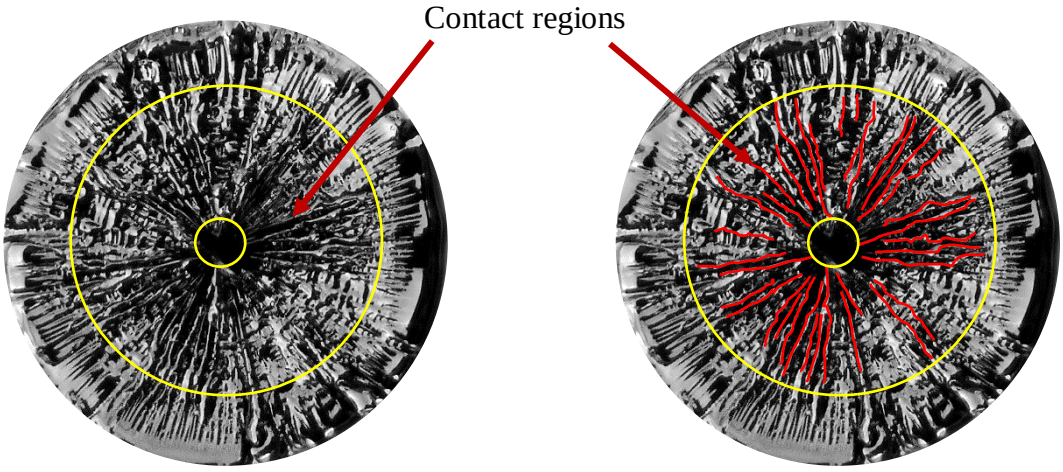

b. Contact regions in cracked area of the asphalt binder

Figure 10. Typical cross section images of the asphalt binder under a strain-controlled rotational shear load

Therefore, calculated true radius or crack length as well as measured true radius or crack length can be obtained based on theoretical formula and image processing, respectively. Figure 11 presents calculated values and measured values of unmodified asphalt binders at 5%, 20°C and 10 Hz. Three observations can be drawn from Figure 11: (1) calculated true radius are larger than measured true radius during the loading process, and the opposite is true for crack length; (2) a good agreement between calculated values and measured values can be observed during the initial and later loading process; and (3) the difference value between calculated values and measured values increases with the increase of loading time until it reaches the peak (first stage in Figure 11a and 11b). Then, it decreases with the increase of loading time (second stage in Figure 11a and 11b).

The calculated values are not exactly consistent with the measured values in this research. It is caused by the existence of the contact regions in Figure 10b, and these contact regions can bear torque. Therefore, three reasons are given for the three observations: (1) the reason why calculated true radius are larger than measured true radius is that a part of strain energy is dissipated by friction among these contact regions. The dissipated strain energy which used to calculate the crack length contains the strain

energy dissipated by these contact regions; (2) the reason for observation 2 is that fewer contact regions make the calculated values and the measured values match well during the initial and later loading process. The reasons for the small proportion of contact regions is that contact regions start to germinate during the initial loading process as well as the uncracked area decreases and torque is transferred to the weaker contact regions during the later loading process, which accelerates the failure of contact regions; and (3) the reason why the difference value has two stages is that contact regions have two change stages. First stage: contact regions increase with the increase of loading time before the difference value reached the peak value; and second stage: contact regions decrease with the increase of loading time after the difference value reached the peak value. Besides, a similar result is found in the polystyrene and polyethylene. T*he "drop-like shape" crack* and contact regions are formed and proved when performing a time sweep test (Mattes et al., 2008).

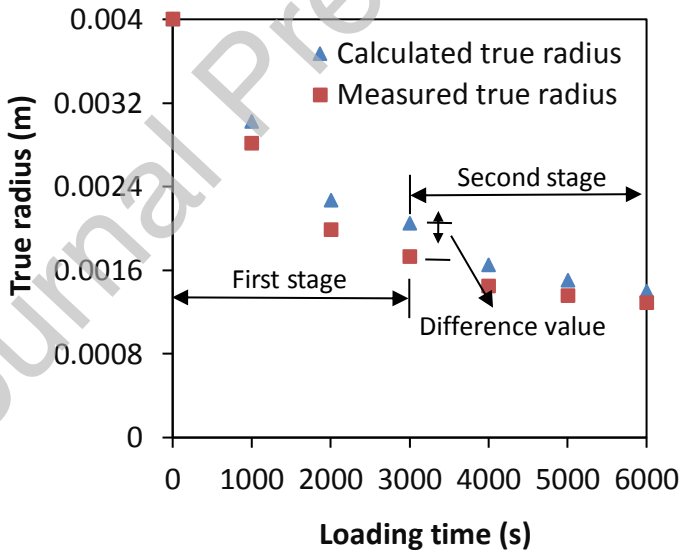

a. Calculated and measured true radius

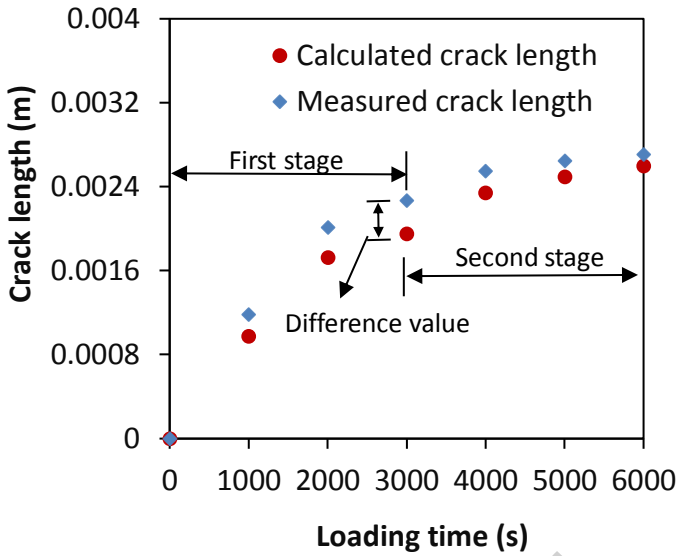

b. Calculated and measured crack length

Figure 11. Calculated and measured true radius or crack length of unmodified asphalt binders at 5%, 20°C and 10 Hz

5.2 Determination of Crack Growth Rate for Asphalt Binders

Paris' law is the most widely used model to characterize crack growth rate of materials (Paris and Erdogan 1963), which relates crack growth to the stress intensity factor or the J-integral. For the viscoelastic materials, large-scale yielding of crack growth occurs. Schapery (1984) proposed that substituting the pseudo J-integral for the stress intensity factor or the J-integral. Therefore, the pseudo J-integral Paris' law is adopted to predict the crack growth rate for asphalt binders, as shown in Equation 26.

$$\frac{dc}{dt} = A\left(J_R\right)^n \tag{26}$$

where A and n *are Paris's law parameters associated with the evolution of crack growth,* and J_R is the pseudo J-integral, which represents the energy dissipation rate caused by damage, which can be calculated as below:

$$J_R = \frac{\partial\left[\int_0^t DPSE^A(t)dt\right]}{\partial\left(V^c\right)} = \frac{\partial\left[\int_0^t DPSE^A(t)dt\right]/\partial t}{\partial\left(V^c\right)/\partial t} = \frac{DPSE^A(t)}{\partial\left(V^c\right)/\partial t} \tag{27}$$

in which $DPSE^A(t)$ is $DPSE^A$ at any loading time t; V^c is the crack volume of the asphalt binder, which calculated by the following expression:

$$\frac{\partial V^c}{\partial t} = 2\pi h r^T \frac{\partial c}{\partial t} \tag{28}$$

The $DPSE^A(t)$ can be determined as follows:

$$DPSE^A(t) = \iiint_{V^A} DPSE^A(t,r,z) \tag{29}$$

Then, substitute Equation 27, Equation 28, Equation 29 into Equation 26 and arrange it, yielding:

$$\frac{dc}{dt} = A^{1/(n+1)} \left[\frac{1}{4} \pi r^A \left| G^{*T} \right|^{1/4} \left(\gamma_0^A \right)^2 \left| G^{*A} \right|^{3/4} \sin\left(\delta^A - \delta_{NLVE}^A \right) \right]^{n/(n+1)} \tag{30}$$

in which δ_{NLVE}^A is the apparent phase angle at the nonlinear viscoelastic critical point of the asphalt binder, which is identified in the section 3.

Next, take the logarithm of both sides of Equation 30, whose result is:

$$\ln\left(\frac{dc}{dt}\right) = \frac{1}{n+1} \ln A + \frac{n}{n+1} \ln\left[\frac{1}{4} \pi r^A \left| G^{*T} \right|^{1/4} \left(\gamma_0^A \right)^2 \right] + \frac{n}{n+1} \ln\left[\left| G^{*A} \right|^{3/4} \sin\left(\delta^A - \delta_{NLVE}^A \right) \right] \tag{31}$$

However, Equation 31 only applies to the stable stage of crack growth. It is necessary to determine the stable stage of crack growth for asphalt binders in this study. Based on the test data and calculation results, Figure 12a presents two stages (unstable crack growth stage and stable crack growth stage) of crack growth of asphalt binders: (1) in unstable crack growth stage: the inverse of true radius slowly increases (crack length rapidly increase) with increases of loading time, which is caused by unstable flow at the edge of asphalt binder sample when performing a strain-controlled rotational shear load; (2) in stable crack growth stage: the inverse of true radius linearly increases with the increase of loading time, which indicates the unstable flow of the edge of the asphalt binder disappears and crack stably growth. In addition, unmodified asphalt binders are presented as an example. Figure 12b shows relationship between the inverse of true radius and loading time in the stable crack growth stage at different oscillation shear strain levels (5%,6%,7%), 20°C and 10 Hz. Results show that a linear relationship between the inverse of true radius and loading time is presented, and high values of goodness of fit are obtained (R^2>0.99). The similar results are obtained in other

conditions or other asphalt binders.

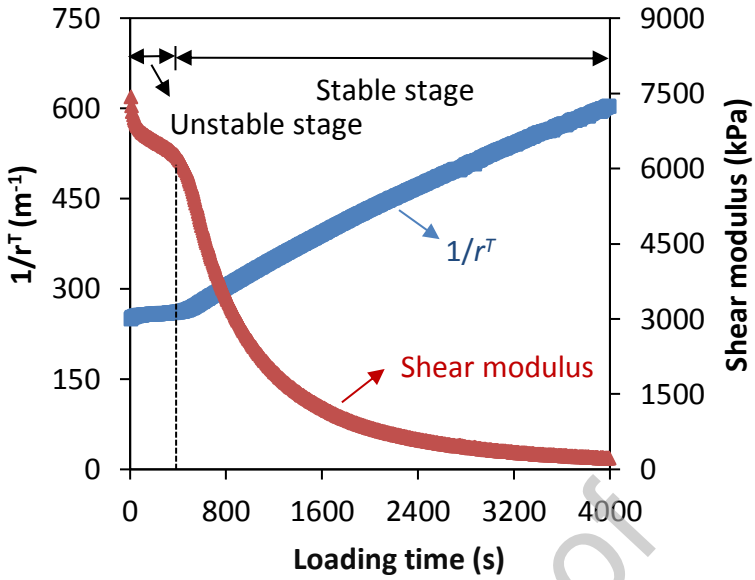

a. Two stages of crack growth

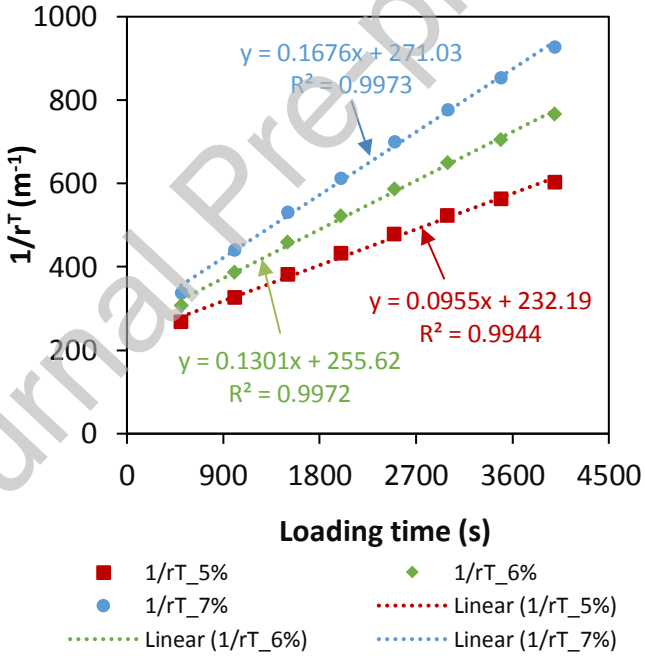

b. Relationship between the inverse of true radius and loading time in stable crack growth stage at different oscillation shear strain levels, 20°C and 10 Hz

Figure 12. Unstable crack growth stage and stable crack growth stage of unmodified asphalt binders

Therefore, the inverse of true radius $\frac{1}{r^T}$ in stable crack growth stage can be expressed by the following linear equation:

$$\frac{1}{r^T} = k_1 t + k_2 \tag{32}$$

where, k_1, k_2 are fitting parameters.

Take the partial derivative of $\frac{1}{r^T}$ to the loading time t:

$$-\left(\frac{1}{r^T}\right)^2 \frac{dr^T}{dt} = k_1 \tag{33}$$

Substitute Equation 25 into Equation 33, the crack growth rate can be determined as follows:

$$\frac{dc}{dt} = \frac{d\left(r^A - r^T\right)}{dt} = -\frac{dr^T}{dt} = k_1\left(r^T\right)^2 \tag{34}$$

Figure 13 presents some examples of plotting crack growth rate and the function of material properties (shear modulus and phase angle) in double logarithm scale under different oscillation shear strain levels and temperatures. 20_5% standing for the test temperature is 20°C and the oscillation shear strain level is 5%, and other legends have similar interpretations. Two conclusions can be drawn from Figure 13: (1) crack growth rate and the function of material properties (shear modulus and phase angle) in double logarithm scale is linear under different oscillation shear strain levels and temperatures, because of high goodness of fit (R^2>0.999); (2) crack growth rate increases with increase the function of material properties (shear modulus and phase angle) in double logarithm scale, that is slopes of these straight lines are positive. In addition, the slopes are almost identical under different oscillation shear strain levels and temperatures.

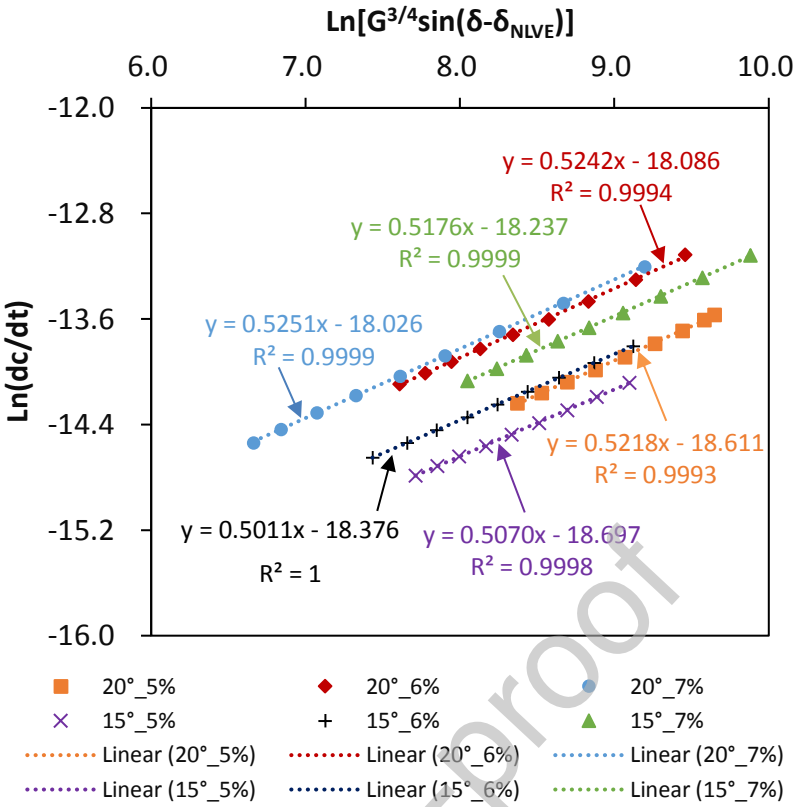

Figure 13. Relationship of crack growth rate and the function of material properties (shear modulus and phase angle) in double logarithm scale under different oscillation shear strain levels and temperatures

Finally, Paris's law parameters n and *A* can be determined by the slope and intercept in Figure 13. Table 6 presents *Paris's law parameters n* and *A* of unmodified asphalt binders and SBS modified asphalt binders at different oscillation shear strain levels and different temperatures. It is found that *Paris's law parameters n* and *A* do not significantly vary with oscillation shear strain levels and temperatures regardless of unmodified asphalt binders or SBS modified asphalt binders. For example, six *Paris'* law parameters *n* of unmodified asphalt binder are approximately equal to 1.10 at 5%, 6%, 7% of oscillation shear strain level when test temperatures are 15°C and 20°C. *Therefore, Paris's law parameters n* and *A* are independent on oscillation shear levels and temperatures. Thus, *n* and *A* can be determined by one oscillation shear strain level and temperature. Then, it can be used to characterize crack growth rate of asphalt binders at any oscillation shear strain level and temperature.

Table 6. *Paris's law parameters of unmodified asphalt binders* and SBS modified asphalt binders at different oscillation shear strain levels and different temperatures

Materials	Oscillation shear strain level	*Paris's law parameters*			
		20℃		15℃	
		n	*A*	*n*	*A*
Unmodified asphalt binders	5%	1.09	4.17E-13	1.05	4.08E-13
	6%	1.10	8.00E-13	1.03	9.93E-13
	7%	1.10	6.41E-13	1.10	4.86E-13
SBS modified asphalt binders	7%	1.51	2.77E-17	1.54	7.97E-18
	8%	1.58	1.83E-17	1.57	7.61E-18
	9%	1.57	2.68E-17	1.63	2.98E-18

6. Conclusions

Targeting the challenge that accurately characterizing the fatigue cracking process of the asphalt binder. An energy-based mechanics approach is applied to determine the crack length and crack growth rate is modeled by the pseudo J-integral in this study. The main findings of this study are listed as follows:

- The linear viscoelastic critical strain level separating linear viscoelasticity from nonlinear viscoelasticity, and the nonlinear viscoelastic critical strain level separating nonlinear viscoelasticity from damage are determined. Results of unmodified asphalt binders as an example, the linear viscoelastic critical strain level is 0.3% and the nonlinear viscoelastic critical strain level is 0.7%.
- A theoretical formula of crack length is derived based on a pure mechanical method. The crack length of asphalt binders can be determined by true shear modulus, apparent shear modulus and apparent radius. Crack length increases and growth rate decreases with the increase of loading time, and larger oscillation shear strain level can increase crack length under the same conditions.
- Contact regions in cracked area of asphalt binders are formed and a part of strain energy is dissipated by friction among these regions when performing a strain-

controlled rotational shear load. In addition, there are two change stages of contact regions, which first increase and then decrease with the increase of loading time.

- Crack growth rate is modeled by the pseudo J-integral Paris' law which considering nonlinear viscoelasticity. Linear relationship between crack growth rate and the function of material properties (shear modulus and phase angle) in double logarithm scale is proven. Slopes of these straight lines are positive and almost identical under different oscillation shear strain levels and temperatures.
- *Paris' law* parameters (*A* and *n*) associated with the evolution of crack growth are determined. They are independent on oscillation shear strain levels and temperatures, which indicate that they are inherent material properties for asphalt binders.

Acknowledgements

This work was supported by Changsha University of Science & Technology via Open Fund of National Engineering Laboratory of Highway Maintenance Technology (grant number KFJ180104).

References

1. Anderson, D. A., & Kennedy, T. W. (1993). Development of SHRP binder specification (with discussion). *Journal of the Association of Asphalt Paving Technologists, 62*.
2. Anderson, D. A., Le Hir, Y. M., Marasteanu, M. O., Planche, J. P., Martin, D., & Gauthier, G. (2001). Evaluation of fatigue criteria for asphalt binders. *Transportation Research Record*, *1766*(1), 48-56.
3. China, M. (2010a). Standard test method for ductility of bitumen: GB/T 4508-2010.
4. China, M. (2010b). Standard test method for penetration of bitumen: GB/T 4509-2010.
5. China, M. (2011). Standard Test Methods of Bitumen and Bituminous Mixtures for Highway Engineering: JTG E20-2011.
6. China, M. (2014). Standard test method for softening point of bitumen-Ring-and

ball apparatus: GB/T4507-2014.

7. Gao, Y., Li, L., & Zhang, Y. (2020). Modeling Crack Propagation in Bituminous Binders under a Rotational Shear Fatigue Load using Pseudo J-*Integral Paris' Law*. *Transportation Research Record*, 2674(1), 94-103.
8. Ghuzlan, K. A., & Carpenter, S. H. (2000). Energy-derived, damage-based failure criterion for fatigue testing. *Transportation research record*, 1723(1), 141-149.
9. Hicks, R. G., Finn, F. N., Monismith, C. L., & Leahy, R. B. (1993). Validation of SHRP binder specification through mix testing (with discussion). *Journal of the Association of Asphalt Paving Technologists*, *62*.
10. Hintz, C., & Bahia, H. (2013). Understanding mechanisms leading to asphalt binder fatigue in the dynamic shear rheometer. *Road Materials and Pavement Design*, *14*(sup2), 231-251.
11. Wang, C., Zhang, H., Castorena, C., Zhang, J., & Kim, Y. R. (2016). Identifying fatigue failure in asphalt binder time sweep tests. *Construction and Building Materials*, 121(SEP.15), 535-546.
12. Kim, Y. R., Lee, H. J., & Little, D. N. (1997). Fatigue characterization of asphalt concrete using viscoelasticity and continuum damage theory (with discussion). *Journal of the Association of Asphalt Paving Technologists*, *66*.
13. Keentok, M., & Xue, S. C. (1999). Edge fracture in cone-plate and parallel plate flows. *Rheologica acta*, *38*(4), 321-348.
14. Li, L., Gao, Y., & Zhang, Y. (2020). Crack length based healing characterisation of bitumen at different levels of cracking damage. *Journal of Cleaner Production*, *258*, 120709.
15. Luo, X., Luo, R., & Lytton, R. L. (2014a). Energy-based mechanistic approach for damage characterization of pre-flawed visco-elasto-plastic materials. *Mechanics of Materials*, *70*, 18-32.
16. Luo, X., Luo, R., & Lytton, R. L. (2014b). Energy-based crack initiation criterion for viscoelastoplastic materials with distributed cracks. *Journal of Engineering*

Mechanics, *141*(2), 04014114.

17. Luo, X., Birgisson, B., & Lytton, R. L. (2020). Kinetics of healing of asphalt mixtures. *Journal of Cleaner Production*, *252*, 119790.
18. Mattes, K. M., Vogt, R., & Friedrich, C. (2008). Analysis of the edge fracture process in oscillation for polystyrene melts. *Rheologica acta*, *47*(8), 929-942.
19. Paris, P., & Erdogan, F. (1963). A critical analysis of crack propagation laws. *Journal of Basic Engineering*, 85(4), 528.
20. Reese, R. (1997). Properties of aged asphalt binder related to asphalt concrete fatigue life. *Journal of the Association of Asphalt Paving Technologists*, *66*.
21. Rowe, G. M., & Bouldin, M. G. (2000). Improved techniques to evaluate the fatigue resistance of asphaltic mixtures. In *2nd Eurasphalt & Eurobitume Congress Barcelona* (Vol. 2000).
22. Safaei, F., & Castorena, C. (2017). Material nonlinearity in asphalt binder fatigue testing and analysis. *Materials & Design*, S0264127517307566.
23. Schapery, R. A. (1984). Correspondence principles and a generalized J integral for large deformation and fracture analysis of viscoelastic media. *International Journal of Fracture*, *25*(3), 195-223.
24. Shan, L., Tian, S., He, H., & Ren, N. (2017). Internal crack growth of asphalt binders during shear fatigue process. *Fuel*, *189*, 293-300.
25. Shen, S., Airey, G. D., Carpenter, S. H., & Huang, H. (2006). A dissipated energy approach to fatigue evaluation. *Road materials and pavement design*, *7*(1), 47-69.
26. Shen, S., Chiu, H. M., & Huang, H. (2010). Characterization of fatigue and healing in asphalt binders. *Journal of Materials in Civil Engineering*, *22*(9), 846-852.
27. Subhy, A., Presti, D. L., & Airey, G. (2017). New simplified approach for obtaining a reliable plateau value in fatigue analysis of bituminous materials. *Engineering Failure Analysis*, *79*, 263-273.
28. Zhang, Y., & Gao, Y. (2019). Predicting crack growth in viscoelastic bitumen under a rotational shear fatigue load. *Road Materials and Pavement Design*, 1-20.

29. Zhou, F., Mogawer, W., Li, H., Andriescu, A., & Copeland, A. (2012). Evaluation of fatigue tests for characterizing asphalt binders. *Journal of Materials in Civil Engineering*, *25*(5), 610-617.

CRediT author statement

Hui Li: Conceptualization, Formal analysis, Investigation, Methodology, Validation, Writing - original draft, Writing - review & editing. **Xue Luo:** Funding acquisition, Supervision, Resources, Project administration, Writing - review & editing. **Weizhuo Yan：** Investigation, Methodology. **Yuqing Zhang:** Supervision, Writing - review & editing.